Transonic Flow about a Thick Circular-Arc Airfoil

John B. McDevitt,* Lionel L. Levy Jr.,† and George S. Deiwert‡
NASA Ames Research Center, Moffett Field, Calif.

An experimental and theoretical study of transonic flow over a thick airfoil is presented. This study was prompted by a need for adequately documented experiments that could provide rigorous verification of viscous-flow simulation computer codes. Test results are presented for Reynolds numbers (based on airfoil chord length) ranging from 1 million to 17 million, covering laminar to fully developed turbulent flows. By varying the airfoil peak local Mach number from about 1 to 1.4, both weak and strong shock boundary-layer interactions were observed. Measurements presented include surface pressures, streamline and flow separation patterns, and shadowgraphs. For a limited range of freestream Mach numbers the airfoil flowfield was found to be unsteady. Instantaneous pressure measurements and high-speed shadowgraph movies were taken to investigate this phenomenon. Comparisons of experimentally determined and numerically simulated steady flows using a new viscous-turbulent code are also included. The comparisons show the importance of including an accurate turbulence model. When the shock-boundary-layer interaction is weak the turbulence model employed appears adequate, but when the interaction is strong, and extensive regions of separation are present, the model is inadequate and needs further development.

Nomenclature

b	= airfoil span
C_p	= pressure coefficient
c	= airfoil chord, $c = 20.3$ cm (8 in.)
$\bar{f}$	= reduced frequency, 2π(frequency)$(c/2)/$(freestream velocity)
h	= half-height of channel
M	= Mach number
P_o	= total pressure
$Re_{c,\infty}$	= Reynolds number based on airfoil chord and freestream conditions
t	= airfoil thickness or time
x	= streamwise coordinate measured from airfoil leading edge
y	= lateral coordinate measured from test channel centerline
z	= vertical coordinate measured from model centerline
Δp	= (instantaneous pressure)-(mean static pressure)
$\Delta()$	= incremental quantity

Subscripts

∞	= freestream conditions
s	= conditions immediately in front of shock
peak	= peak value

Superscript

*	= conditions at sonic velocity

Introduction

THE full potential of advanced computers will not be realized in aerodynamic applications until adequate models are found for the turbulent transport. A new viscous-turbulent code, employing the complete Navier-Stokes equations, and with application to the transonic flow over airfoils, is currently under development by Deiwert[1,2] at the Ames Research Center and the present experimental study was undertaken in support of this code development.

Although numerous investigations have been made of viscous effects on airfoils, and many studies made of separated flow phenomena in general (e.g., Refs. 3–9), the information available is not completely suitable for guiding the development or viscous-turbulent computer codes. Often, the test Reynolds number range is too low and the separation phenomena are sometimes subject to large and uncertain wall interference effects, test-flow nonuniformity, and angle-of-attack effects. Ideally, an experimental transonic airfoil study would involve the simplest geometry possible, and include both trailing-edge and shock-induced separations. This paper describes such an experiment. A new facility was constructed and the airfoil and test-section geometry specifically chosen so as to achieve the desired test program.

First, a brief description of the new facility, the Ames high Reynolds number channel, is given. Next, the first experimental tests conducted in the new facility are described and the results presented and discussed. The paper then concludes with comparisons of measured and numerically simulated transonic airfoil pressure distributions using recent results from the viscous-turbulent code being developed at Ames.

Facility

The new facility is of the blow-down type and uses a large settling tank with various throttling plates and screens for conditioning the flow. The facility is designed for operation at reynolds numbers per foot up to 40 million for subsonic flows and to 200 million for supersonic flows. Interchangeable test-channel configurations are used, each designed specifically for the test flow to be studied.

For the present study a test channel 25 cm wide, 38 cm high, and 150 cm long (10x15x60in.) was chosen with the airfoil spanning the channel (see Fig. 1). The design of the bellmouth entrance section for this test section is described in Ref. 10. The test Mach number was regulated by choking the flow downstream of the test section, either by the use of inserts in the upper and lower channel walls, or in combination with a translating two-dimensional wedge, as shown in Fig. 1. Although the wedge operates in the wake of the test airfoil, extensive tests indicated that the wedge did not affect the test results (a conclusion reached by comparing airfoil pressure distributions obtained with and without the use of the wedge). Also incorporated in the design of the upper and lower test-section-channel walls were removable inserts contoured to

Presented as Paper 75-878 at the AIAA Fluid and Plasma Dynamics Conference, Hartford, Conn., June 16-18, 1975: submitted June 27, 1975: revision received December 5, 1975. The helpful suggestions made by Joseph G. Marvin are hereby acknowledged.

Index categories: Subsonic and Transonic Flow; Nonsteady Aerodynamics.

*Research Scientist, Experimental Fluid Dynamics Branch. Associate Fellow AIAA.

†Research Scientist, Experimental Fluid dynamics Branch. Member AIAA.

‡Research Scientist, Computational Fluid Dynamics Branch. Member AIAA.

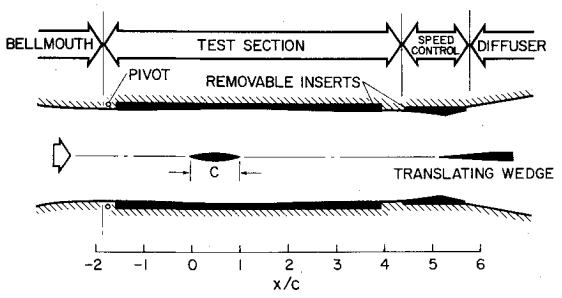

Fig.1 Test section schematic.

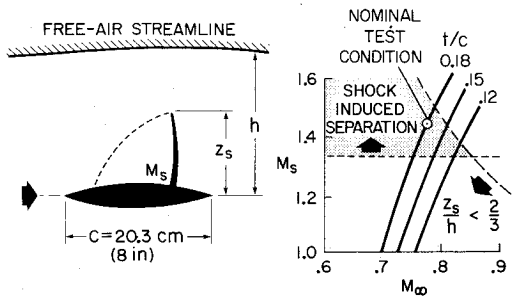

Fig.2 Biconvex circular-arc airfoil experiment.

simulate the flow streamlines about the airfoil in free air at the chosen design Mach number and Reynolds number, an effective means for eliminating wall interference effects. The upper and lower walls were also hinged at their leading edges to provide minor adjustments to compensate for displacement effects of the channel boundary layer, and for use at other than the nominal test condition.

Basic Considerations

Since the primary intent of the study was to provide basic data to guide the further development of computer codes, the simplest of airfoils was chosen – the circular-arc profile, which is characterized by a constant radius of curvature. The numerical method of Ref. 1 was used to compute the inviscid transonic flow about a family of circular-arc airfoils and the experimental program was then chosen on the basis of the results shown in Fig. 2.

To eliminate upper and lower wall interference effects, and to prevent premature choking of the tunnel by the transonic airfoil shock, these walls were contoured to follow the airfoil free-air streamlines for the chosen nominal test condition. The side wall interference effects were minimized by the choice of a nonlifting experiment and by specifying beforehand that the experimental program be restricted to flows where the ratio of shock height to channel width (the wing planform aspect ratio is not the important parameter here) is less than one half, which, for the channel used, required that $z_s/h<2/3$. Consideration was also given to the belief that the local Mach number ahead of the shock should reach at least 1.35 to insure that the important shock-induced boundary-layer separation phenomenon could be included in the study. These considerations led to the choice of an 18% thick airfoil, a nominal test Mach number of 0.775 (as indicated in Fig. 2), and the test section shown in Fig. 1.

For the present tests the upper and lower channel walls were each diverged 0.15 deg (see pivot point in Fig. 1) to account for channel wall boundary-layer growth based on a nominal unit free-stream Reynolds number of 10 million. The inviscid streamline contours for the nominal test Mach number of 0.775 are listed in Table 1.

Model

The ordinates of the stainless steel model were accurate to within ± 0.008 cm, except that the theoretically sharp leading and trailing edges were, by necessity, replaced by cylindrically

Table 1 Upper and lower channel wall contours

x/c	$\Delta z/c$	x/c	$\Delta z/c$
−1.56	0	1.25	0.0334
−1.50	0.0008	1.50	0.0265
−1.25	0.0044	1.75	0.0223
−1.00	0.0079	2.00	0.0196
−0.75	0.0113	2.25	0.0171
−0.50	0.0160	2.50	0.0146
−0.25	0.0238	2.75	0.0121
0	0.0344	3.00	0.0096
0.25	0.0463	3.25	0.0071
0.50	0.0540	3.50	0.0046
0.75	0.0528	3.75	0.0021
1.00	0.0431	3.94	0

blunted edges of approximately 0.002-cm diam. The airfoil pressure orifices were 0.03-cm diam and formed by an electric-arc discharge technique so as to insure sharp edges.

Tests and Procedures

The test data included surface-pressure measurements on the airfoil and channel walls, oil-film studies to display surface streamlines and locate lines of flow separation, and flowfield shadowgraphs. The tests were conducted at free-stream Reynolds numbers, based on airfoil chord length, ranging from 1 million to 17 million. The test Mach number was varied from near the critical value ($M_\infty \approx 0.71$) to the highest possible without the airfoil choking the channel.

Pressure measurements were made along the centerline on both upper and lower airfoil surfaces, and at various spanwise stations on one surface.The results indicated two-dimensional flow over most of the airfoil, the only exception being the regions immediately adjacent to the channel walls. The model was tested in both upright and inverted positions to check flow angularity in the channel; there was none. Surface oil-film studies were also conducted to substantiate the nearly two-dimensional aspects of the tests. Extensive tests were also made to insure that choking the flow at the downstream end of the test channel was an effective freestream Mach number control and did not affect the test results.

The test free-stream (corresponding to $x/c=-\infty$) Mach number was obtained as follows: The local Mach number at the side wall of the channel directly ahead of the wing at station x/c=-1.34 (see Fig. 1) was evaluated from measurements of total pressure and wall static pressure. The Mach number in the center of the channel was then obtained by correcting for the variation in local Mach number across the channel. This was determined from flow calibration runs to be approximately $\Delta M=0.003$. The freestream Mach number was then evaluated from an empirical relationship

$$\frac{M_\infty}{M_{x/c=-1.34}} = 1.016 + 0.140(M_{x/c=-1.34} - 0.7)$$

derived from numerical calculations using the method described in Ref. 1 for the test airfoil in free air at Mach numbers between 0.7 and 0.8.

The basic pressure measuring system employed transducers located outside the channel and the response time (to reach 99.9% of the true value) was of the order of 2 sec. All pressure transducers were calibrated immediately before each test run. Error analyses indicated pressure measurements were accurate to ± 0.1% of the channel total pressure. Approximately 10 – 15 sec were required to start the flow in the channel and reach the desired test condition. The flow was then held steady at constant P_0, M_∞ for a minimum of 5 sec and the airfoil and channel wall pressures recorded simultaneously.

During the course of the investigation it was discovered (from viewing high-speed shadowgraph movies of the flowfield) that unsteady oscillatory flow occurred for certain combinations of Reynolds number and Mach number. To

Table 2 Location of Kuhlite transducers for dynamic pressure measurements

Transducer	Location
A	Channel sidewall forward of airfoil, $x/c=-1.34, z/c=-0.375$
B	Channel sidewall downstream of airfoil, $x/c=3.16, z/c=-0.375$
1_U	Airfoil upper surface, $x/c=0.50$, $(y/b)/2=0.70$
1_L	Airfoil lower surface, $x/c=0.50$, $(y/b)/2=0.70$
2_U	Airfoil upper surface, $x/c=0.775$, $(y/b)/2=0.70$
2_L	Airfoil lower surface, $x/c=0.775$, $(y/b)/2=0.70$

provide detailed information in this unsteady flow regime, four miniature pressure sensors were located directly in the airfoil with the transducer diaphragms within 2 mm of the airfoil surface (response time less than 10^{-3}sec). Similar sensors were also flush-mounted in the channel walls to determine if a coupling existed between the unsteady flow about the airfoil and the channel test Mach number. The test data indicated that none existed. The exact locations of these transducers are described in Table 2.

Results and Discussion

A major concern in a test program of the present type is the possibility that three-dimensional effects would seriously degrade the data. Comparisons of steady-flow pressure measurements at several spanwise stations are made in Fig. 3. Two examples are presented for a relatively low Reynolds number where the airfoil boundary layer was believed to be laminar for the most part (based on comparisons of pressure distributions obtained with and without boundary-layer trips at the airfoil leading edge) and two examples for a well-established turbulent layer (Figs. 3c and 3d). These data indicate that the flows were essentially two-dimensional; the only appreciable deviation occurred nearest the wall for the data in Fig. 3a. Pressure measurements along the centerlines of the contoured upper and lower walls are also included in Fig. 3. (The measured C_p values at the walls rapidly approached zero both upstream and downstream of the airfoil).

Typical photographs of oil-film patterns and shadowgraphs of the aft flowfield are presented in Fig. 4 for trailing-edge separation and in Fig. 5 for separation at the base of the shock wave (shock-induced separation). The oil-film patterns also indicate the absence of signficant three-dimensional effects.

Representative test results, which illustrate Reynolds number effects when the flow is steady (except close to the trailing edge for the lowest Reynolds number), are presented in Figs. 6 and 7. At $M_\infty \approx 0.750$ the pressure recovery over the aft portion of the airfoil is large and boundary-layer separation occurs near $x/c=0.9$, as indicated by oil-film patterns. (A typical separation pattern was included in Fig. 4.) At $M_\infty \approx 0.780$ the aft pressure recovery is weak and shock-induced separation occurs (an example of shock-induced separation was displayed in Fig. 5). The flowfield is directly affected by the displacement effect of the boundary layer and the effect of changes in Reynolds number on peak pressure coefficient, shock strength, shock location, and aft pressure recovery are appreciable, particularly at low Reynolds numbers. In general, the Reynolds number effect is small for numbers above 10 million.

Representative test data obtained at constant Reynolds number are displayed in Fig. 8 to demonstrate Mach number

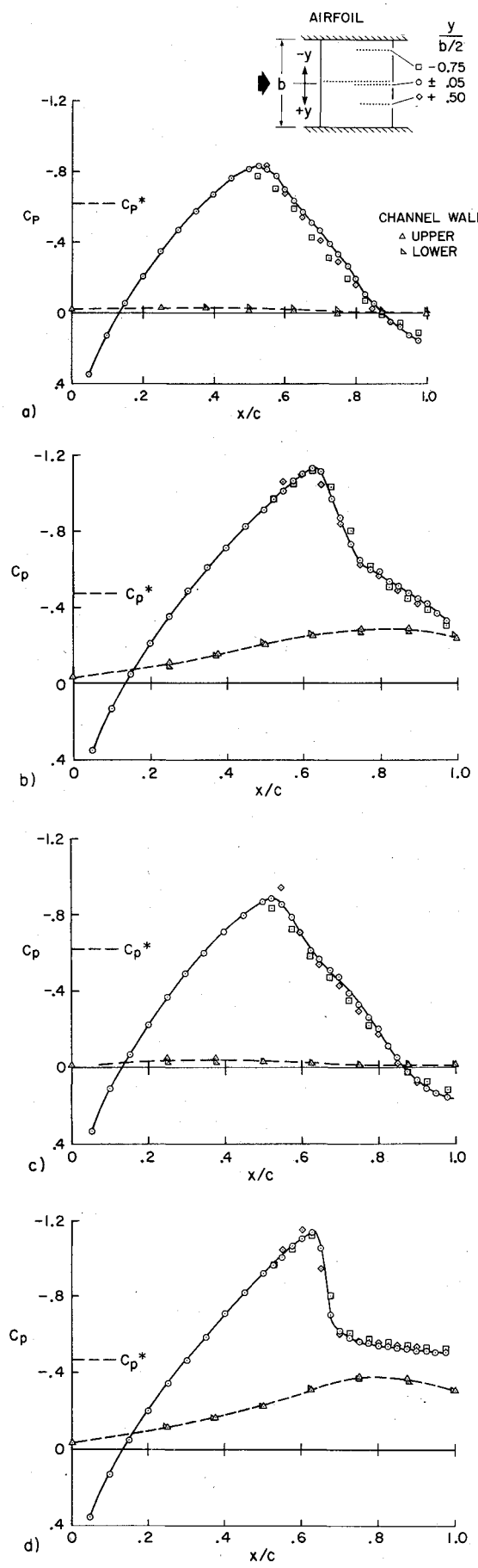

Fig.3 Pressure distributions on airfoil and upper and lower channel walls; a) $Re_{c,\infty}=2.1\text{x}10^6$, $M_\infty=0.743$; b) $Re_{c,\infty}=2.1\text{x}10^6$, $M_\infty=0.786$; c) $Re_{c,\infty}=10.3\text{x}10^6$, $M_\infty=0.741$; d) $Re_{c,\infty}=10.3\text{x}10^6$, $M_\infty=0.786$.

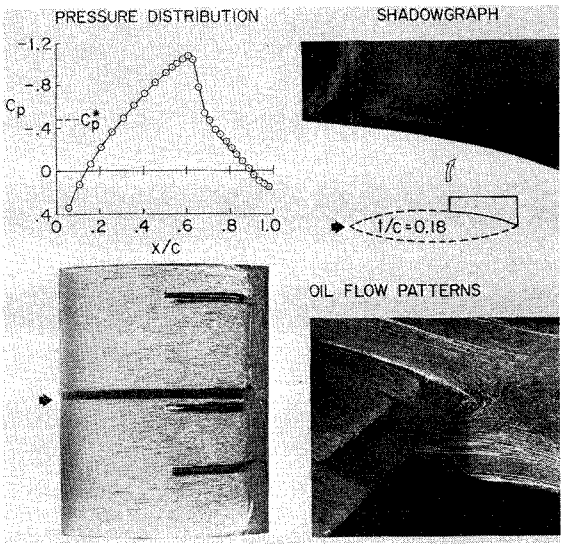

Fig.4 Trailing-edge boundary-layer separation, $Re_{c,\infty} = 10.3 \times 10^6$, $M_\infty = 0.760$.

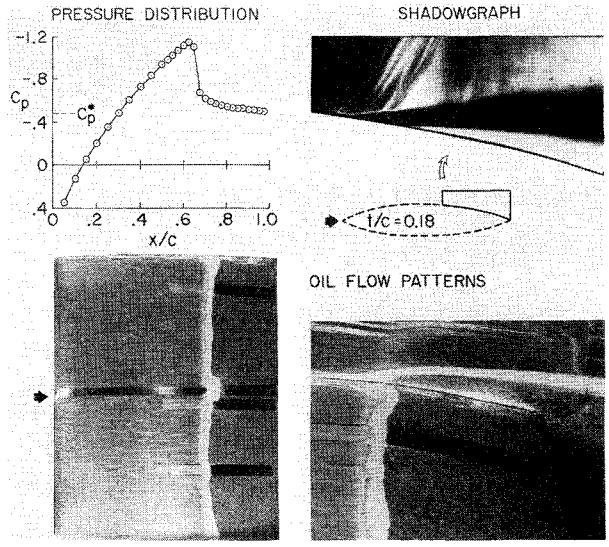

Fig.5 Shock-induced boundary-layer separation, $Re_{c,\infty} = 10.3 \times 10^6$, $M_\infty = 0.786$.

effects. Included in this figure are variations of the parameters $C_{p_{x/c=0.975}}$ (a convenient measure of aft surface pressure recovery) and M_{peak} (local Mach number at peak C_p) with M_∞. As the test Mach number is increased above the critical value ($M_{\text{peak}} = 1$), steady flow with strong aft pressure recovery, and with boundary-layer separation located near the trailing edge ($x/c \approx 0.9$), persists for the test Reynolds number range (1 million to 17 million) until approximately $M_\infty = 0.76$. Then, as the freestream Mach number is increased from about 0.76 to 0.78, the flow is unsteady (to be discussed subsequently). About $M_\infty \approx 0.78$ the flow is again steady (except for the lowest Reynolds number of 1 million), with separation now fixed at the base of the shock wave.

In the unsteady-flow regime the parameters $C_{p_{x/c=0.975}}$ and M_{peak} vary more or less smoothly with increasing M_∞ for Reynolds numbers of about 4 million, or less. For Reynolds numbers above about 5 million the variations are difinitely discontinuous, and double values were obtained, indicating the presence of a hysteresis phenomenon (to be discussed in more detail later).

High-speed shadowgraph movies were made of the flow over the aft portion of the airfoil as the free-stream Mach number was varied from 0.740 to 0.785. (The translating speed-control wedge shown in Fig. 1 was used to increase the

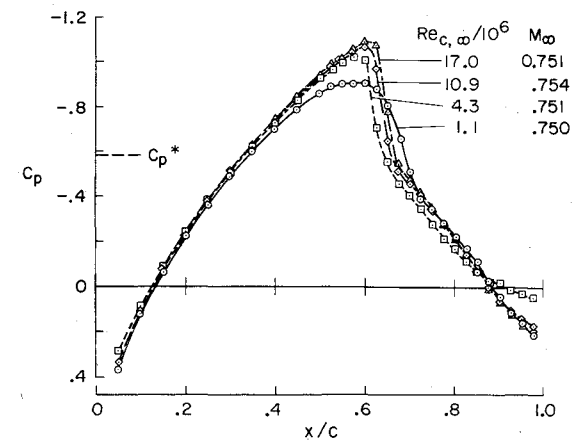

Fig.6 Reynolds number effect, $M_\infty \approx 0.750$.

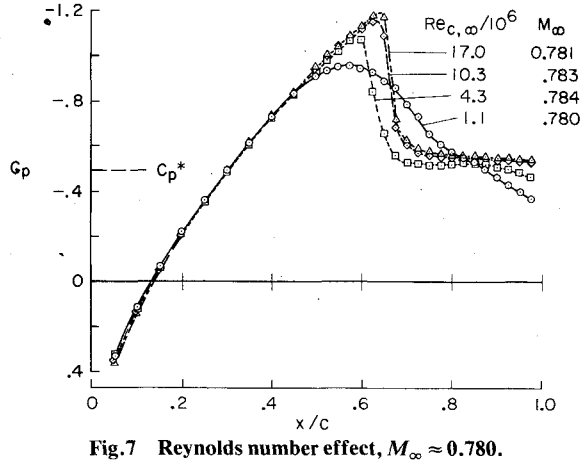

Fig.7 Reynolds number effect, $M_\infty \approx 0.780$.

free-stream Mach number during filming at a rate of $dM_\infty/dt \approx 0.002$/sec.) Photographs of selected frames from a movie for a test run at $Re_{c,\infty} = 7.3 \times 10^{-6}$ are shown in Fig. 9. Initially, for free-stream Mach numbers less than about 0.76, the flow was steady with separation near the trailing edge (upper photograph in Fig. 9). (The three curved lines along the upper portion of the window are oil streaks and should be ignored.) At $M_\infty \approx 0.76$ the flow became unsteady, with the separation line oscillating between a location near the trailing edge to the base of the shock wave. As the Mach number increased, the periodic motion of the boundary layer and shock wave persisted until approximately $M_\infty = 0.78$, where the flow field again appeared to be steady but with separation now fixed at the base of the shock wave.

To obtain detailed information concerning this unsteady flow phenomenon, instantaneous pressure measurements were obtained with transducers placed in the airfoil at $x/c = 0.5$ and 0.775 (upper and lower surface) and at the sidewall of the channel (see Table 2). The reference sides of these differential transducers were connected by tubing of sufficient volume to provide damping (response time of about 3 sec) to adjacent pressure orifices at the same streamwise location. Selected oscillograph traces of pressure fluctuations obtained as the Mach number was continuously increased from 0.740 to 0.785 are shown in Fig. 10 for $Re_{c,\infty} = 7.3 \times 10^6$. The periodic unsteadiness is an asymmetric phenomenon as the airfoil upper surface pressure measurements 1_U (at $x/c = 0.5$) and 2_U (at $x/c = 0.775$) are exactly 180 deg out of phase with the opposing lower surface measurements (traces 1_L and 2_L).

The onset of unsteady flow is almost instantaneous (Fig. 10a) and the mean level of the pressure traces is shifted momentarily as the reference side of the transducers adjust to a new mean level (see Fig. 8d). As the free-stream Mach number increases (Fig. 10b) the pressure fluctuations diminish in

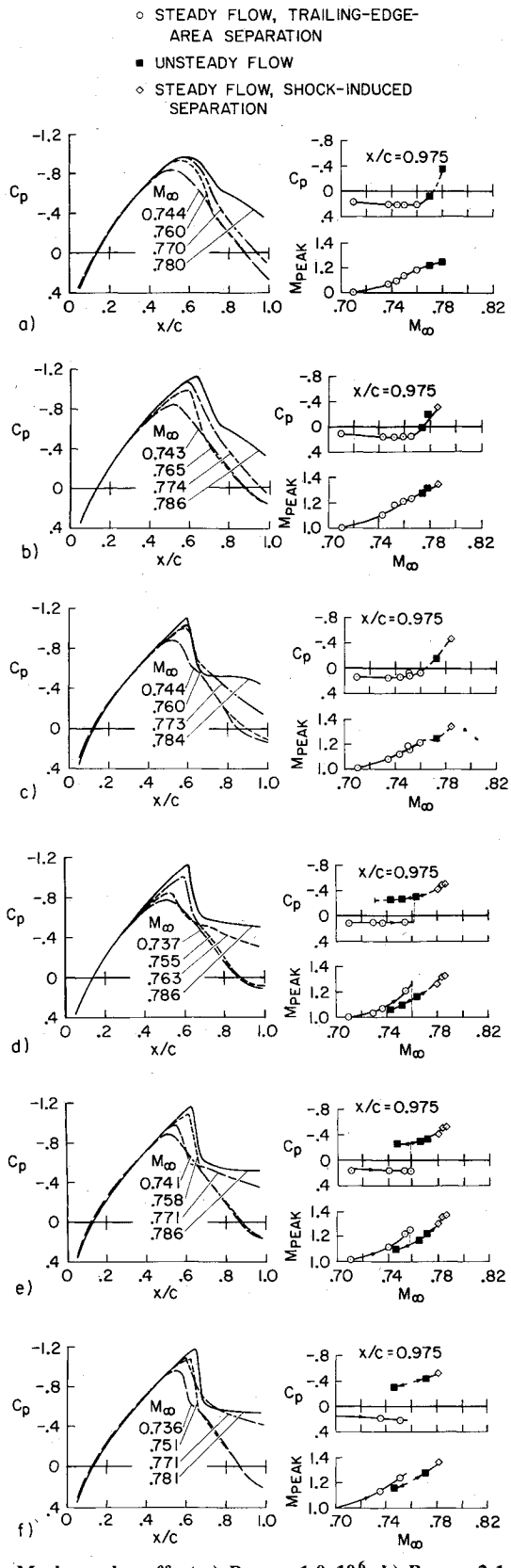

Fig.8 Mach number effect:a) $Re_{c,\infty} = 1.0\text{x}10^6$; b) $Re_{c,\infty} = 2.1\text{x}10^6$; c) $Re_{c,\infty} = 4.3\text{x}10^6$ d) $Re_{c,\infty} = 7.3\text{x}10^6$; e) $Re_{c,\infty} = 10.3\text{x}10^6$; f) $Re_{c,\infty} = 17.0\text{x}10^6$.

amplitude and steady flow is indicated at $M_\infty = 0.780$ (separation is now fixed at the base of the shock wave). The upstream sidewall measurement (trace A) does not noticeably change at the onset of unsteady flow and is an indication of the noise level of the tunnel.

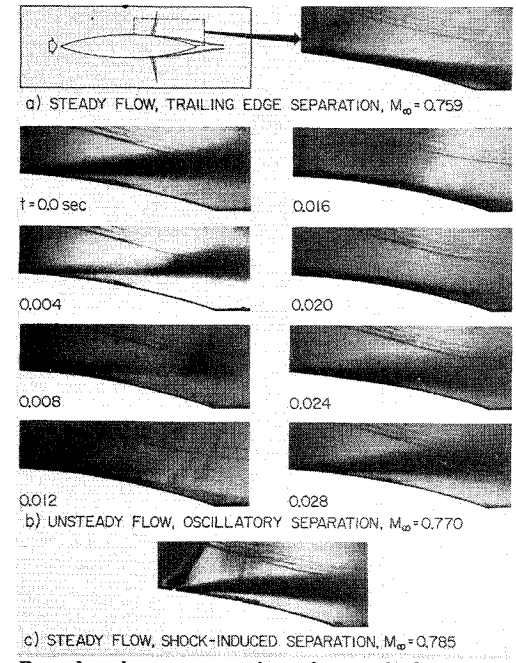

Fig.9 Boundary-layer separation from shadowgraph movie, $Re_{c,\infty} = 7.3\text{x}10^6$.

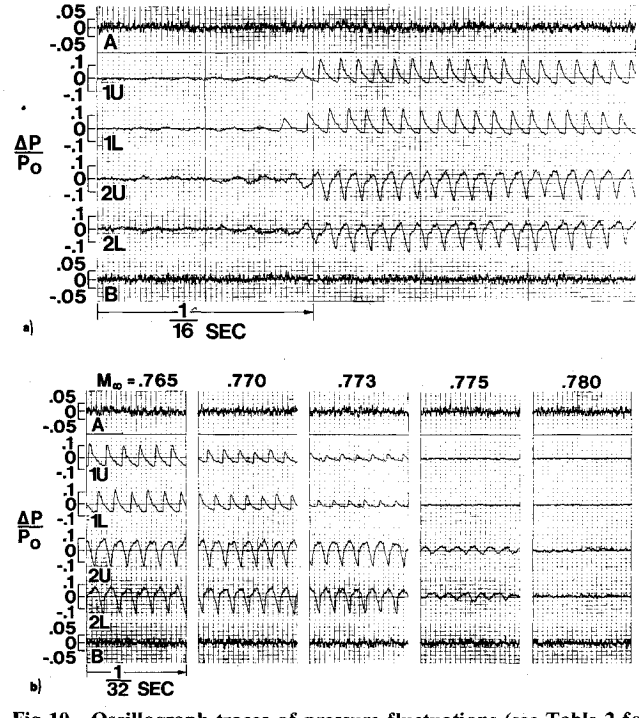

Fig.10 Oscillograph traces of pressure fluctuations (see Table 2 for sensor locations), $Re_{c,\infty}$ 7.3x10^6: a) Onset of unsteady flow, $M_\infty = 0.760$; b) $M_\infty = 0.765$ to 0.780.

A few cycles of oscillograph measurements at the airfoil upper surface, recorded just after the onset of unsteady flow, are displayed in Fig. 11 in a manner that shows the fluctuations in pressure coefficient. Also shown in this figure are crude estimates of the envelopes of the pressure fluctuations, based on the two dynamic measurements made. The surprisingly large pressure excursions might be explained on the basis of the large boundary-layer displacement effects shown in Fig. 9b. To determine if a coupling existed between the airfoil oscillatory flow phenomena and the channel flow, the signals were also recorded on magnetic tape and post-run spatial cross correlations of signal A (channel sidewall ahead of the airfoil where the local Mach number for steady flow is within

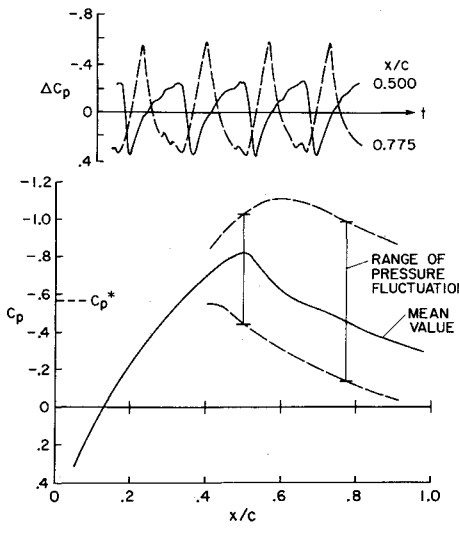

Fig.11 Pressure fluctuations at onset of unsteady flow, $M_\infty = 0.760, Re_{c,\infty} = 7.3 \times 10^6$.

2% of M_∞) with the airfoil measurements were made. Correlation coefficients of approximately 0.1 were obtained for both steady and unsteady flows. The numbers obtained were below the threshold for a meaningful interpretation and it was concluded that no coupling existed between the airfoil oscillatory flow phenomena and the oncoming channel flow. The extreme rigidity of the airfoil and test channel should preclude a structural resonate phenomenon, and power spectral density analyses of signal A demonstrated this to be the case.

The frequency of the periodic motion shown in Fig. 10a was approximately 188 Hz (the frequency cannot be deduced from the successive motion-picture frames presented in Fig. 9 because the camera framing rate was only slightly greater than the cyclic rate of the unsteady flow).

Since the separation alternates between the trailing-edge and shock-induced phenomena, large changes in displacement effects occur and the unsteady motion may be explained on that basis. For example, if the local Mach number ahead of the shock is near the critical value for shock-induced separation, and if shock-induced separation suddenly occurs on the upper surface while the lower surface separation is near the trailing edge, the effective airfoil profile is no longer symmetrical and the effect of the negative camber is to slow down the flow over the upper surface. This tends to suppress the shock-induced phenomenon but, at the same time, to induce higher velocities over the lower surface, thus promoting the shock-induced phenomenon there, and the flow fields reverse. When the free-stream Mach number is increased to a value sufficiently above the critical, the oscillatory behavior ceases and both surfaces experience steady, shock-induced separation.

Oscillograph traces similar to those presented in Fig. 10 were obtained at Reynolds numbers from 5 million to 17 million. For $Re_{c,\infty} < 4 \times 10^6$, pressure fluctuations were observed primarily at $x/c = 0.775$. Typical measurements at a low Reynolds number (where the boundary layer is believed to have been transitional) are presented in Fig. 12. The frequencies of the periodic measurements were within 190 ± 3 Hz for the Reynolds number range from 1 million to 17 million (the reduced frequency f was approximately 0.49).

A recent study of unsteady transonic airfoils by Finke[11] included tests of a 20% thick circular-arc airfoil at $\alpha = 0$ deg and the unsteady shock oscillation appeared at a slightly lower Mach number, $M_\infty = 0.71$, which is to be expected for the thicker profile. The airfoil chord length was varied but the reduced frequency remained constant at $f \approx 0.51$ and it was, therefore, concluded that the shock oscillation was not caused by tunnel effects.

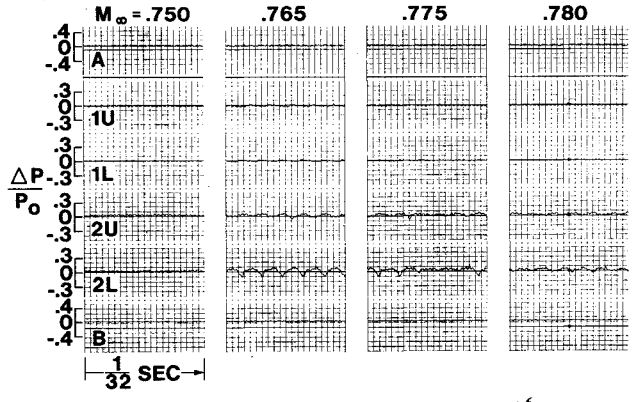

Fig.12 Pressure fluctuations, $Re_{c,\infty} = 2.1 \times 10^6$.

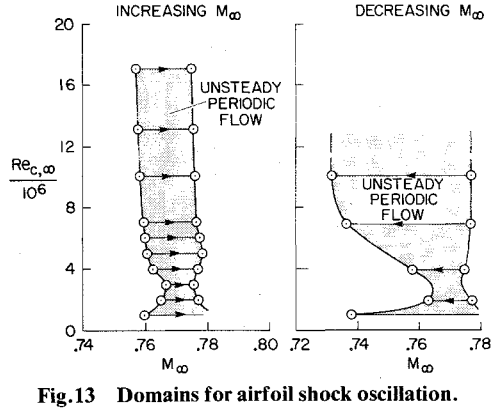

Fig.13 Domains for airfoil shock oscillation.

The Reynolds number, Mach number domains where periodic shock oscillations occur are shown in Fig. 13 for both increasing and decreasing free-stream Mach numbers. (Test runs could not be made at Reynolds numbers greater than about 10 million for decreasing Mach number because the translating speed-control wedge (see Fig. 1) was insufficiently powered.) The right-hand boundaries (Fig. 13) are essentially the same but the left-hand boundaries are considerably different, indicating a strong hysteresis effect, typical of large separation phenomena.

The first appearance of shock-induced separation, and the onset of cyclic flow, occurred near $M_{peak} \approx 1.25$. A discussion of various criteria for predicting separated flows is included in Ref. 12 and, for shock-induced separation on transonic airfoils, Osborne's criterion (see also discussion in Ref. 13) was found to be consistent with the present results. Osborne's purely empirical relationship between the airfoil geometry and the surface local Mach number ahead of the shock (M_{peak}) predicts for the present airfoil a shock-induced separation critical value of 1.22, which is only slightly lower than the experimental value.

Comparisons of Experiment with Numerical Simulations

The present experimental study was undertaken to provide definitive information suitable, in particular, for the evaluation of new viscous turbulent-flow computer codes. Since it is not now feasible for computers to employ a computational mesh size smaller than the lowest scale of turbulence, some way must be found to model the turbulent transport adequately. One effort, by Deiwert, numerically solves the full Navier-Stokes equations. He has recently successfully programmed his method for use on the ILLIAC IV computer. The numerical method is described in Ref. 1 and recent efforts to obtain a turbulence model that will predict the present experimental data are discussed in detail in Ref. 2.

Sample comparisons of numerical solutions from Refs. 1 and 2 with experiment are presented in Fig. 14 (for the viscous

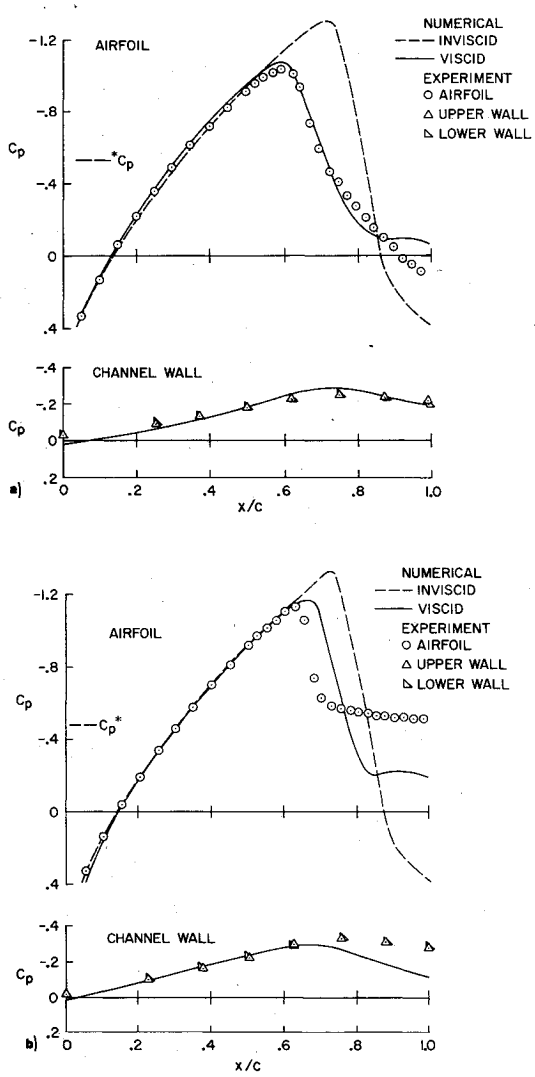

Fig.14 Comparisons of numerical solutions with experiment: a) $M_\infty = 0.775, Re_{c,\infty} = 2\text{x}10^6$; b) $M_\infty = 0.786, Re_{c,\infty} = 10\text{x}10^6$.

solutions, turbulent model 2 of Ref. 2 was used). The inviscid solution agrees remarkably well with experiment over the forward half of the airfoil but is inaccurate in predicting shock strength and location, and in predicting the pressure level near the trailing edge. When the aft pressure recovery is strong, indicating that the shock boundary-layer interaction is weak (Fig. 14a) the viscous solution agrees well with experiment, predicting reasonably well the shock strength and location. The only significant difference appears to be near the airfoil trailing edge, where the experimental pressure distributions do not indicate as extensive a separation region as does the numerical computation. Good agreement between computation and experiment is also obtained at the channel walls, indicating that the streamline contouring used was reasonably accurate and was effective in this case for minimizing wall interference effects.

At the higher Mach number (Fig.14b), where separation is near the foot of the shock wave, the viscous solution does not predict the shock location and strength, and greatly overpredicts the pressure recovery over the aft portion of the airfoil. At the channel walls the agreement between computation and experiment parallels that at the airfoil surface, -upstream of the airfoil shock the agreement is excellent but downstream the numerical method overestimates the pressure recovery and disagrees with experiment. This is probably due, in part, to inadequate turbulent modeling in the vicinity of the separation point and throughout the separated region, and efforts to devise more suitable models are continuing (see discussion in Ref. 2). Also contributing to the disagreement downstream of the shock location was the fact that the channel upper and lower walls were contoured to match an inviscid-flow soluiton at a slightly lower Mach number. The channel wall boundaries should, of course, be the same in both the numerical simulation and experiment for a proper comparison.

Conclusions

The present experimental study of the transonic flow over an 18% thick circular-arc airfoil resulted in a diversity of results: 1) steady flows with either weak or strong shock boundary-layer interactions; 2) either trailing-edge-area or shock-induced separations; 3) unsteady, asymmetric periodic flows involving simple trailing-edge separation; and 4) large-amplitude pressure fluctuations induced by the oscillatory switching of the separation from the trailing-edge area to the base of the shock wave.

The pressure coefficients forward of the airfoil shock are, in the absence of blunt-nose effects, relatively insensitive to changes in Mach number and Reynolds number. The shock boundary-layer interaction phenomena, however, are strongly dependent on Mach number and Reynolds number and the steady-flow data for this simple airfoil are ideally suited for evaluating turbulence modeling. For the case of trailing-edge-area separation, numerical viscous solutions can be found that agree well with experiment, predicting closely the shock strength and location. The only region of relatively poor agreement occurs in the immediate vicinity of the trailing edge. For the strong shock boundary-layer interaction case, recent attempts to devise a suitable turbulence model have shown considerable progress, but as yet no adequate model is available.

Although the intent of the present study was to obtain static data, the unsteady pressure data included in this paper are of interest in their own right, since unsteady flows have long been of interest to aerodynamicists (see, for instance, Ref. 14). If a suitable turbulence model is found for the static case, the dynamic case could, in principle, follow, as time-accurate solutions can be obtained with advanced computers.

This paper presents the first results from an extensive program to document fully the flow over basic airfoil shapes which can be used as a guide for the development of a turbulent transport model that realistically accounts for the physics of the entire flow field. Future measurements will include skin friction, heat transfer, and flow field velocities from a laser-Doppler velocimeter.

References

[1] Deiwert, G.S., "Numerical Simulation of High Reynolds Number Transonic Flow," AIAA Paper 74-603, Palo Alto, Calif., 1974.

[2] Deiwert, G.S., "Computation of Separated Transonic Turbulent Flows," *AIAA Journal*, Vol. 14, June 1976.

[3] Ackeret, J., Feldman, F., and Rott, N., "Investigations of Compression Shocks and Boundary Layers in Gases Moving at High Speeds," NACA TM 1113, Jan. 1947.

[4] Schubauer, G.B. and Klebanoff, PmS., "Investigation of Separation of the Turbulent Boundary Layer," NACA Rept. 1030, 1951.

[5] Knechtel, E.D., "Experimental Investigation at Transonic Speeds of Pressure Distributions over Wedge and Circular-Arc Airfoil Sections and Evaluations of Perforated-Wall Interference," NASA TN D-15, Aug. 1959.

[6] Pearcey, H.H., Osborne, J., and Haines, B., "Interaction between Local Effects at the Shock and Rear Separation," *AGARD Conference Proceedings*, No. 35, Paper 11, Sept., 1968.

[7] Stanewsky, E. and Little, B.H., Jr., "Studies of Separation and Reattachment in Transonic Flow," AIAA Paper 70-541, 1970.

[8] Albers, I.E., Bacon, J.W., Masson, B.S., and Collins, D.J., "An Experimental Investigaiton of Turbulent Transonic Viscous – Inviscid Interactions, *AIAA Journal*, Vol. 11, May 1973, pp. 620-627.

[9] Collins, D.J. and Krupp, J. A., "Experimental and Theoretical Investigations in Two-Dimensional Transonic Flow," AIAA Paper 73-659, Palm Springs, Calif., 1973.

[10]Levy, L.L., Jr. and McDevitt, J. B., "A Design Method for Entrance Sections of Transonic Wind Tunnels with Rectangular Cross Sections," NASA TM X-62,490, May 1975.

[11]Finke, K., "Unsteady Shock-Wave Boundary-Layer Interaction on Profiles in Transonic flow," AGARD-CPP-168, Paper 28, 1975.

[12]Hahn, M., Rubbert, P.E., and Mahal, A.S., "Evaluation of Separation Criteria and Their Application to Separated Flow Analysis," Wright-Patterson Air Force Base, Ohio, AFFDL-TR-72-145, Jan. 1973.

[13]Pearcey, H.H., "Shock-Induced Separation and Its Prevention by Design and Boundary-Layer Control," *Boundary Layer and Flow Control*, Pergamon Press, New York, Vol. 2, 1961, pp. 1166-1344.

[14]Polentz, P.P., Page, W.A., and Levy, L.L., Jr., "Unsteady Normal-Force Characteristic of Selected NACA Profiles at High Subsonic Mach Numbers," NACA RM A55C02, May 1955.

From the AIAA Progress in Astronautics and Aeronautics Series . . .

AEROACOUSTICS: JET AND COMBUSTION NOISE; DUCT ACOUSTICS—v. 37

Edited by Henry T. Nagamatsu, General Electric Research and Development Center; Jack V. O'Keefe, The Boeing Company; and Ira R. Schwartz, NASA Ames Research Center
A companion to Aeroacoustics: Fan, STOL, and Boundary Layer Noise; Sonic Boom; Aeroacoustic Instrumentation, volume 38 in the series.

This volume includes twenty-eight papers covering jet noise, combustion and core engine noise, and duct acoustics, with summaries of panel discussions. The papers on jet noise include theory and applications, jet noise formulation, sound distribution, acoustic radiation refraction, temperature effects, jets and suppressor characteristics, jets as acoustic shields, and acoustics of swirling jets.

Papers on combustion and core-generated noise cover both theory and practice, examining ducted combustion, open flames, and some early results of core noise studies.

Studies of duct acoustics discuss cross section variations and sheared flow, radiation in and from lined shear flow, helical flow interactions, emission from aircraft ducts, plane wave propagation in a variable area duct, nozzle wave propagation, mean flow in a lined duct, nonuniform waveguide propagation, flow noise in turbofans, annular duct phenomena, freestream turbulent acoustics, and vortex shedding in cavities.

541 pp., 6 x 9, illus. $19.00 Mem. $30.00 List

TO ORDER WRITE: Publications Dept., AIAA, 1290 Avenue of the Americas, New York, N. Y. 10019